

## Chemical investigation of hassium (Hs, Z=108)

Ch.E. Düllmann, H.W. Gäggeler, S. Soverna, A. Türler (Univ. Bern & PSI), R. Dressler, B. Eichler, F. Glaus, D.T. Jost, D. Piguet (PSI), T.N. Ginter, K.E. Gregorich, U. Kirbach, D.M. Lee, R. Sudowe, (LBNL), D.C. Hoffman, H. Nitsche, J.B. Patin, P. Zielinski (UC Berkeley & LBNL), W. Brüchle, R. Eichler, E. Jäger, V. Pershina, M. Schädel, B. Schausten, E. Schimpf, H.-J. Schött, G. Wirth (GSI), S.N. Timokhin, A.B. Yakushev (FLNR), K. Eberhardt, P. Thörle, N. Trautmann (Univ. Mainz), Z. Qin (IMP Lanzhou), A. Vahle (FZ Rossendorf)

The heaviest element, whose chemical behavior has been studied so far is bohrium (Bh) with  $Z=107$  [1] behaving like a typical member of group 7 of the periodic table. The longest-lived  $\alpha$ -decaying isotope of the next heavier element hassium (Hs,  $Z=108$ ) is  $^{269}\text{Hs}$  ( $T_{1/2}=11.3$  s) which has been identified in the decay chain of  $^{277}\text{112}$  [2,3]. Hs is supposed to be a member of group 8 of the periodic table and should thus form a very volatile tetroxide. Relativistic density functional calculations predicted the electronic structure of  $\text{HsO}_4$  to be similar to the one of  $\text{OsO}_4$  [4]. Application of different semiempirical models of the interaction of a  $\text{MeO}_4$  molecule with quartz surface predicted the adsorption behavior of  $\text{OsO}_4$  and  $\text{HsO}_4$  to be very similar [4]. Extrapolations of trends within group 8 of the periodic table also predicted  $\text{HsO}_4$  and  $\text{OsO}_4$  to behave similar in a gas adsorption chromatography experiment [5].

Hs isotopes were produced directly in the reaction  $^{248}\text{Cm}(^{26}\text{Mg};5,4n)^{269,270}\text{Hs}$  at the UNILAC at GSI Darmstadt [6]. Hs isotopes recoiling from the target were thermalized and oxidized in a  $\text{He}/\text{O}_2$  mixture in the recoil chamber of the In-situ Volatilization and On-line detection apparatus IVO [7]. Volatile  $\text{HsO}_4$  was transported with the carrier gas to the Cryo-On-Line-Detector (COLD), a thermochromatography device. Along a narrow channel formed of PIN-diodes registering  $\alpha$ -decaying and spontaneously fissioning (SF) nuclides, a temperature gradient from  $-20$  to  $-170$  °C was established. The deposition temperature of volatile species could therefore be determined, allowing for the determination of their adsorption enthalpy. COLD is an improved version of the Cryo-Thermochromatography Separator CTS developed at Berkeley [8].

Five decay chains were detected in the course of the experiment which were attributed to  $^{269}\text{Hs}$  or the so far unknown isotope  $^{270}\text{Hs}$  [6]. In addition, two  $\alpha$ -SF correlations were observed in detectors 3 and 4 that still have a rather low random probability, but could not be assigned with certainty to either  $^{269}\text{Hs}$  or  $^{270}\text{Hs}$  [6]. The deposition temperature of the Hs containing molecules was determined to  $(-44\pm 5)$  °C giving strong evidence of the formation of  $\text{HsO}_4$ . In an irradiation of a  $^{152}\text{Gd}$  target,  $^{172}\text{Os}$  ( $T_{1/2}=19.2$  s) was produced in the reaction  $^{152}\text{Gd}(^{26}\text{Mg};6n)$  and a deposition temperature of  $(-82\pm 5)$  °C was measured for  $^{172}\text{OsO}_4$ . The deposition distribution in the COLD array along the detector pairs is shown in Fig. 1. From these deposition peaks the adsorption enthalpies were deduced applying a Monte-Carlo simulation based on a microscopic description of the transport process in the chromatography column [9], i.e. in the COLD system. Since the half-life of the nuclide is a crucial parameter in this simulation and this value has not yet been measured for  $^{270}\text{Hs}$ , only the three events

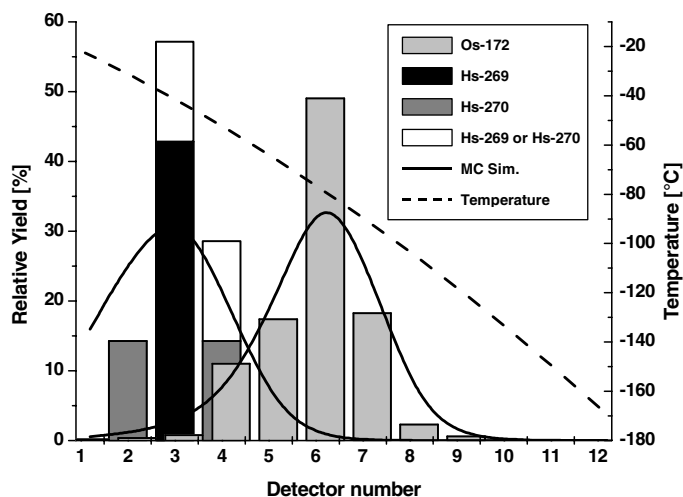


Fig. 1 Merged thermochromatograms of  $\text{OsO}_4$  and  $\text{HsO}_4$ . The solid lines represent results of a Monte-Carlo Simulation with  $\Delta H_{\text{ads}}$  values of  $-39.5$   $\text{kJ}\cdot\text{mol}^{-1}$  ( $\text{OsO}_4$ ) and  $-47$   $\text{kJ}\cdot\text{mol}^{-1}$  ( $\text{HsO}_4$ ), respectively. The dashed line indicates the temperature gradient.

assigned to  $^{269}\text{Hs}$  were used for the simulation.  $\Delta H_{\text{ads}}(\text{HsO}_4)=(-47\pm 2)$   $\text{kJ}\cdot\text{mol}^{-1}$  (68 % c.i.) was evaluated, compared to  $\Delta H_{\text{ads}}(\text{OsO}_4)=(-39.5\pm 1.0)$   $\text{kJ}\cdot\text{mol}^{-1}$ . The latter value is in good agreement with  $\Delta H_{\text{ads}}(\text{OsO}_4)=(-38.0\pm 1.5)$   $\text{kJ}\cdot\text{mol}^{-1}$  evaluated in earlier experiments.

With the formation of a very volatile oxide, presumably  $\text{HsO}_4$ , Hs behaves similar to Os, its next lighter homologue in group 8 of the periodic table.

## References

- [1] R. Eichler et al., *Nature* **407**, 63 (2000).
- [2] S. Hofmann et al., *Z. Phys.* **A354**, 229 (1996).
- [3] S. Hofmann et al., *Rev. Mod. Phys.* **72**, 733 (2000).
- [4] V. Pershina et al., *J. Chem. Phys.* **115**, 792 (2001).
- [5] Ch.E. Düllmann et al., *J. Phys. Chem. A* (submitted)
- [6] A. Türler et al., this Annual Report and submitted to *Phys. Rev. Lett.*
- [7] Ch.E. Düllmann et al., *Nucl. Instrum. Meth.* **A479**, 631 (2002).
- [8] U. Kirbach et al., *Nucl. Instrum. Meth. A* (in press)
- [9] I. Zvara et al., *Radiochim. Acta* **38**, 95 (1985).

# Confidence Intervals for Experiments with Background and Small Numbers of Events

W. Brüche, GSI

Some nuclear reactions with low cross sections yield only small numbers of atoms or specific events. It is not trivial to give statistically satisfying error bars for this cross sections and derived constants like e.g. fission branches or chemically interesting  $K_d$ - values. The right description for low count rates is given by the Poisson distribution (see Fig. 1 and Formula 1).

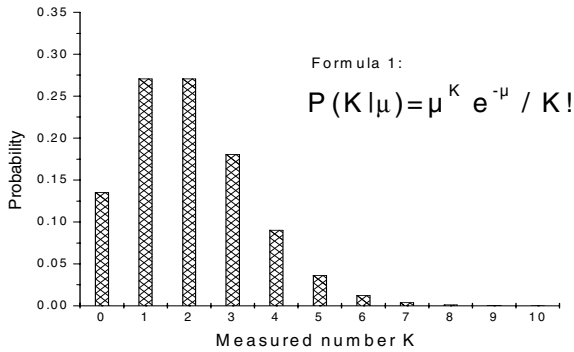


Fig.1 Poisson distribution for mean expectation number  $\mu=2$

But often one does not know  $\mu$ , but measures  $K$  events and wants to know the mean  $\mu$  and its error. Classically the lower and upper limits  $\mu_l$  and  $\mu_u$  are given by the following equations (for a 'central' interval with equal errors on both sides)[1,2] :

$$1 - \sum_{K=0}^{K_m-1} \frac{\mu_l^K}{K!} e^{-\mu_l} = \epsilon/2 \quad \sum_{K=0}^{K_m} \frac{\mu_u^K}{K!} e^{-\mu_u} = \epsilon/2 \quad (2)$$

with  $\epsilon=0.32$ , corresponding to the conventional  $1\sigma$  error of a Gaussian, and  $K_m$  the observed number.  $\mu_l$  and  $\mu_u$  are determined by iteration. Another method is the so called Bayesian. If one covers all possible values of  $\mu$ , weighing with the probability of  $\mu$  to give an observation of  $K$ , one shall get a probability density distribution of likely  $\mu$ 's. If one integrates the resulting curve to get a central interval, the upper limit is identical with the classical value, but the lower value differs. The reason is the limit  $K_m-1$  in formula 2. To show that this limit yields wrong results one can perform the gedanken experiment to set  $\epsilon=1$  (confidence level zero). Then  $\mu_l$  and  $\mu_u$  are expected to have identical values with 50% of all probabilities below and above this value. This is only the case when  $K_m-1$  in formula 2a is replaced by  $K_m$ . Now the results are the same as with the Bayes method. From Fig. 2 one can see there is some flaw with the central interval. For skewed curves the central method with equal error probability on both sides cuts at different probability densities (horiz. pattern). For the extreme case  $k=0$ , when no event was observed, the central method would even cut off the part with the highest probability. To overcome these difficulties it is recommended to switch to the 'shortest interval' with the highest probability density (vertical pattern). Here the 'middle' interval contains the same area in both cases.

Let us now consider the case of non-negligible background, e.g. from contaminating nuclides, electronic noise, or cosmic

showers. Normally these background rates are Poisson distributed, too. It would be wrong to subtract just the mean background rate (BG) from the measured value and go on with the above-mentioned method. One reason for this is, that normally the average BG is no integer number, but our basis is, that only integer numbers (counts) are measured. It is wrong, too, to shift the Poisson curve for the measured  $K$  by the value of BG, since this would result in negative count-rates for parts of the distribution. The actual background is restricted to values of less than or equal to the measured value  $K$ . First, one has to determine the distribution of background values with formula 1 and  $\mu=BG$ , and has to normalize to 100% for background values between zero and the measured  $K$ ; cutting off all possible background contributions higher than the measured value that naturally is the sum of the unknown real events and the unknown actual background. Then one can sum up all Poisson curves for the possible real value, weighing with the probability of  $(K-\text{background})$ . Fig. 3 shows an example for measured  $K=3$  and  $BG=1.2$ . The method can be expanded to ratios of small numbers.

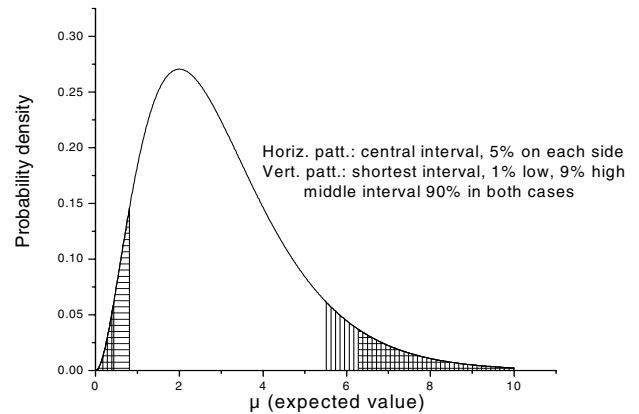


Fig. 2 Poisson distribution for measured  $K=2$

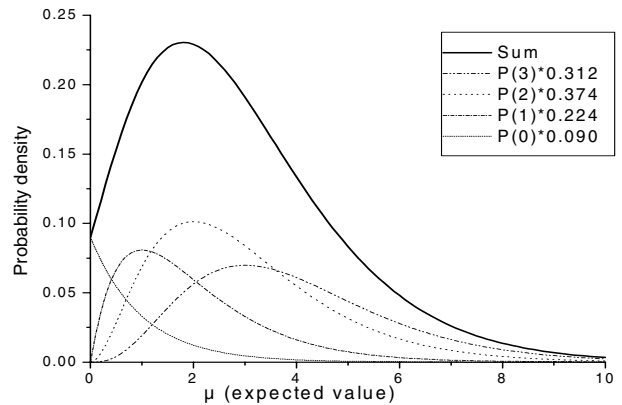


Fig. 3 Probability density for  $K=3$  and  $BG=1.2$

[1] K. H. Schmidt et al., Z. Phys. A 316 (1984) 19-26  
 [2] Biometrika Tables for Statisticians Vol. 1, 3.ed. 1966

## Deposition of osmium tetroxide on reactive surfaces

A. von Zweidorf<sup>1,2</sup>, R. Angert<sup>1</sup>, W. Bröchle<sup>1</sup>, E. Jäger<sup>1</sup>, J.V. Kratz<sup>2</sup>, G. Langrock<sup>2</sup>, M. Mendel<sup>2</sup>, A. Nähler<sup>2</sup>, M. Schädel<sup>1</sup>, B. Schausten<sup>1</sup>, E. Schimpf<sup>1</sup>, E. Stiel<sup>1</sup>, N. Trautmann<sup>2</sup>, G. Wirth<sup>1</sup>

<sup>1</sup>Gesellschaft für Schwerionenforschung, Darmstadt, <sup>2</sup>Institut für Kernchemie, Johannes Gutenberg-Universität Mainz

The recent study of the chemistry of element 108, hassium [1], leads to the conclusion, that it forms a volatile oxide, as expected for a member of group 8 of the periodic table [2]. So far, no chemical reaction of this oxide is known. To learn more about the chemical behaviour of hassium, one would like to investigate the chemistry of hassium oxide, the only known compound of hassium. Presumably, it is chemically similar to OsO<sub>4</sub> and RuO<sub>4</sub>, which have an acidic character and are able to form salts with alkaline materials.

For that reason, a Continuously Working Arrangement For Clusterless Transport Of In-situ Produced Volatile Oxides, CALLISTO, was developed and successfully used to deposit the volatile OsO<sub>4</sub> on metallic sodium surfaces [3]. Although these surfaces are very efficient for the deposition process, the quality of the  $\alpha$ -spectra deteriorates with time. This could be explained by the obvious fact, that the sodium surface is covered with an increasing oxide layer, which doesn't interfere significantly with the deposition process, but disturbs considerably the detection process. Consequently, other deposition materials are required.

It is well known, that OsO<sub>4</sub> reacts with olefins. Mostly this reaction is done in solution. For purposes of  $\alpha$ -detection, a solid olefin with the ability to form a smooth layer would be required.

Fortunately, cis-1,4-polybutadiene is such a substance. It contains double bonds and because of its polymeric character one can easily produce reproducible layers of it. (Fig. 1)

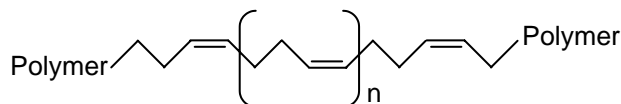


Fig. 1: cis-1,4-polybutadiene

The yield of the reaction of the solid polymer with the gaseous OsO<sub>4</sub> is shown in Fig. 2.

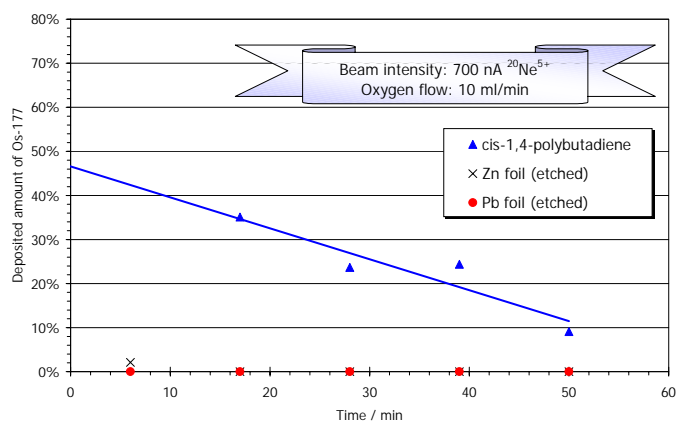


Fig. 2: Deposition of osmium tetroxide on cis-1,4-polybutadiene

Unfortunately, this relatively low yield shows, that this method is not adequate for experiments with hassium oxide. As shown,

cis-1,4-polybutadiene is more reactive than etched surfaces of zinc and lead, on which almost nothing is deposited.

This leads to the implication, that alternative materials for the deposition of OsO<sub>4</sub> are needed.

If alkaline materials are suitable for our purposes, an alkaline surface would be most efficient. Unfortunately, it is hardly possible to reproducibly prepare thin layers of an alkali hydroxide without a substrate. Nevertheless, is it possible to coat an inert material with a smooth layer of alkali hydroxide. We choosed at first graphite as inert substrate and coated it with a thin layer of KOH, using the solubility of KOH in C<sub>2</sub>H<sub>5</sub>OH and preparing the layer from an ethanolic solution. The results for 2 different amounts of helium as transport gas are shown in Fig. 3.

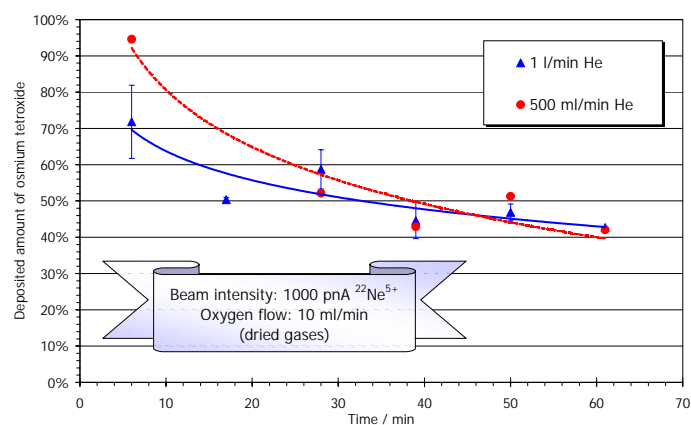


Fig. 3: Deposition of OsO<sub>4</sub> on graphite, coated with KOH

We used our recently developed gas drying-unit to dry the transport gases, remaining less than 0.5 ppm humidity in the gas flow. Surprisingly, the yield of the deposited OsO<sub>4</sub> decreases significantly with time. This behaviour is relatively unexpected, because the macroscopic amount of hydroxide cannot be fully neutralised with the microscopic amount of osmium tetroxide.

In a recent experiment, we found evidence for the important role of catalytic amounts of water. If we add some additional water vapour to the transport gas, the deposition process benefits greatly. This could explain, why an alkaline surface would be less reactive after a certain time of contact with the dried gas. This has to be studied in a forthcoming experiment.

We want to thank Dr. M. Watson, MPI Mainz, for the preparation of cis-1,4-polybutadiene.

[1] <http://www.gsi.de/presse/Hassium.html>

[2] V. Pershina *et al.*, J. Chem. Phys. **115** (2001), p.792

[3] A. v. Zweidorf, GSI Scientific Report 2000-1, p.171

## Preparation of Targets for the New GSI Rotating Wheel Target Assembly

K. Eberhardt<sup>1</sup>, P. Thörle<sup>1</sup>, N. Trautmann<sup>1</sup>, M. Schädel<sup>2</sup>, E. Schimpf<sup>2</sup>  
<sup>1</sup>Institut für Kernchemie, Universität Mainz; <sup>2</sup>GSI, Darmstadt

Electrodeposition is widely used for the preparation of lanthanide and actinide targets on metallic and non-metallic backing materials.[1] For heavy ion studies often Be is required as backing material. The deposition of lanthanide and actinide elements can be performed from an organic solution (usually isopropanol) with current densities of only a few mA/cm<sup>2</sup> and voltages up to 1200 V. The lanthanide or the actinide compound, normally the nitrate, is dissolved in a small volume (5-20 µl) of 0.1 N nitric acid and then mixed with 7 ml of the organic solvent. With this „Molecular Plating (MP)“ technique target densities in the order of 1 mg/cm<sup>2</sup> are possible.

In order to prevent excessive heating of a stationary target at high beam currents as delivered from heavy-ion accelerators, a rotating wheel system with a multi-target device has been developed at GSI. Here, the rotation speed of the wheel is adapted to the pulse structure of the ion beam. The wheel rotates with a frequency of 2000 rpm in order to distribute each beam pulse evenly over one target segment.

A multi-target device consists of three banana-shaped segments. One segment is shown schematically in Fig. 1. The target area is 1.9 cm<sup>2</sup> per segment and the banana-shaped backing is mounted on a Al-frame prior to deposition.

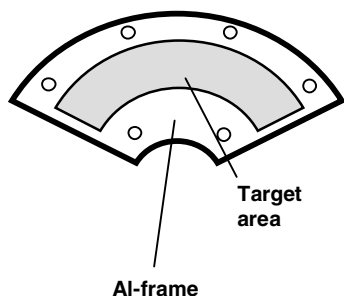


**FIGURE 1.** Schematic view of one of three segments for a rotating wheel target arrangement. The banana-shaped target covers an area of 1.9 cm<sup>2</sup> (per segment).

Table 1 summarizes the lanthanide and actinide targets produced in the last two years at the Institut für Kernchemie in Mainz for the new GSI rotating wheel target assembly. The <sup>248</sup>Cm targets have been used in a recent experiment at GSI to investigate the chemical properties of hassium (Z=108) [2]. Here, a 2.82 mg/cm<sup>2</sup> Be foil was used as backing material. The <sup>248</sup>Cm targets were irradiated with an intense <sup>26</sup>Mg<sup>5+</sup>-beam with an energy of 192.7 MeV applying beam currents up to 6.6 µA. The <sup>248</sup>Cm target material was obtained by chemical separation from a <sup>252</sup>Cf-source [3]

Very often, prior to deposition, chemical separation procedures are required to ensure highest possible purity of the target material. This is of special importance in many HI-experiments, since HI-reactions with impurities like Pb have much higher cross sections compared to the HI-reaction of the target material itself. Furthermore, traces of Be present in recycled

target material, prevent an effective deposition by molecular plating, and thus must be removed.

For this, the irradiated target material is dissolved in 2 N nitric acid from the Be backing foil and the solution is evaporated to dryness. The residue is dissolved in 2 ml of a nitric-acid/methanol mixture (1 N HNO<sub>3</sub>/90 Vol% methanol). This solution is transferred to an anion-exchanger column (AIX; BIORAD AG 1X8) and the column is eluted with 4 x 2 ml of the methanolic solution at room temperature. Under these conditions, Be is completely removed from the column. In the next step the trivalent lanthanides or actinides are eluted with 1 N nitric acid. This procedure is repeated at least twice to get rid of all Be.

**Table 1.** Targets used in HI reaction experiments with the new GSI rotating wheel assembly.

Isotope	Backing	Thickness [µg/cm <sup>2</sup> ]	Method
Ba (nat)	Ti / 5 µm	400	MP
Ce (nat)	Ti / 5 µm	800	MP
Nd (nat)	Ti / 5 µm	800	MP
Gd (nat)	Be / 10 µm	1100	MP
Dy (nat)	Ti / 5 µm	800	MP
Er (nat)	Ti / 5 µm	800	MP
Yb (nat)	Ti / 6 µm	300	MP
U(nat)/Nd(nat)	Be / 10 µm	800	MP
Gd-152	Be / 10 µm	800	MP
<sup>#</sup> Cm-248	Be / 15 µm	240	MP
	Be / 15 µm	730	MP
	Be / 15 µm	690	MP

<sup>#</sup> 3 segments form a complete target device

Pb and other impurities are separated from lanthanide or actinide elements by means of a cation-exchanger column (CIX; Dowex 50WX8). 3 ml of a 0.5 N HCl solution are transferred to a CIX-column (150 x 4 mm) operated at 55°C. The column is first washed with 8 x 2 ml 0.5 N HCl. Then Pb is eluted with 10 ml 1.5 N HCl and 5 ml 1.5 N HNO<sub>3</sub>, whereas the trivalent lanthanides and actinides remain on the column. In a subsequent step, the lanthanides or the actinides are eluted with 15 ml 8 N HNO<sub>3</sub>. This procedure is repeated with a smaller column (50 x 3 mm).

### References:

- [1] K. Eberhardt et al., AIP Conference Proceedings **576**, 1144 (2001)
- [2] Ch. E. Düllmann et al.; to be submitted to Nature
- [3] R. Malmbeck et al., Radiochim.Acta **89**, 543 (2001)

# Vacuum thermochromatography of radon on transition metals Cu, Ag, Au, Pd, and Ni

R. Eichler, E. Jäger, E. Schimpf & M. Schädel (GSI Darmstadt)

Already in 1975, Pitzer [1] suggested that superheavy elements 112 and 114 may behave chemically like noble gases. Contrary to this assumption, 112 and 114 may behave similar to their homologues in groups 12 and 14, Hg and Pb, respectively, but with a much more noble character [2,3].

Assuming a noble gas like behavior of the elements 112 and 114, the chemically most similar element is Rn, a so-called pseudo-homologue to 112 and 114. A differentiation between a noble gas and a noble metal can be done using gas adsorption chromatographic techniques with metal surfaces as stationary phases. As a model study, we investigated adsorption properties of Rn on transition metal surfaces of Cu, Ag, Au, Ni, and Pd. We choose the method of vacuum thermochromatography. It provides several crucial advantages: (i) no carrier gases = no surface contamination, no co-adsorption effects, (ii) excellent heat isolation = stable temperature gradients to 20 K, (iii) fast separation, (iv) comfortable coupling to physical separators, working at vacuum conditions or at low gas pressures.

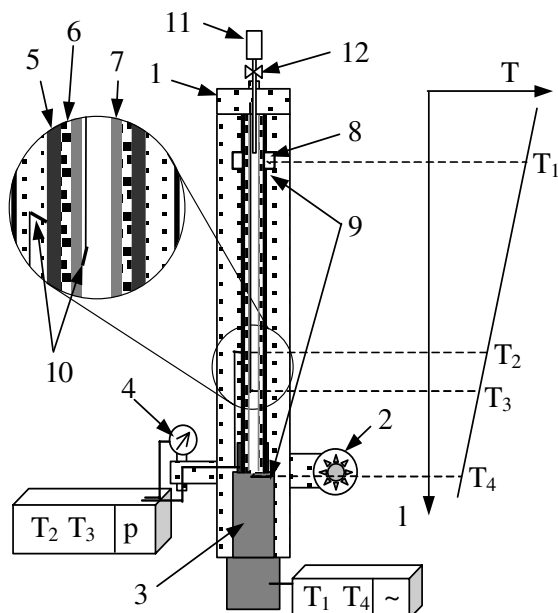


**Figure 1.** Schematic view of the vacuum thermochromatography setup and the temperature gradient with: **1** vacuum chamber, **2** turbo molecular pump, **3** cryogenic pump, **4** ionization gauge, **5** copper tube ( $\varnothing_i = 5$  mm) mounted onto the cryogenic pump head, **6** quartz tube ( $\varnothing_i = 3.75$  mm), **7** metal foil inlay, **8** oven, **9** thermocouples controlling the temperature gradient ( $T_1$  temperature of the cryogenic pump,  $T_4$  oven temperature), **10** monitoring thermocouples ( $T_2$  stationary, on the outside of the copper tube,  $T_3$  inside, moveable along the column), **11** emanation source of  $^{220}\text{Rn}$  or  $^{219}\text{Rn}$  ( $^{232}\text{ThO}_2$ ,  $^{227}\text{Ac}_2\text{O}_3$ ), **12** valve.

Vacuum thermochromatography has been used already in the 1970's at the mass separator OSIRIS [4,5] and for adsorption investigations of heavy actinides [6] and Po [7]. However, for the first time we have installed and operated a low temperature vacuum thermochromatography. Fig. 1 shows a schematic of the device built at GSI.

Off-line vacuum chromatography experiments are performed in the following way. After evacuating the entire set-up to  $3 \times 10^{-5}$  Pa, the valve (12) to the Rn-source (11) is opened. Rn isotopes emanate into the chromatography column. They undergo thousands of adsorption-desorption steps along the chromatography column until they decay to their long-lived decay products  $^{212}\text{Pb}$  and  $^{211}\text{Pb}$ . The Pb atoms keep adsorbed at low temperatures, and thus, they are not moving along the chromatographic surface. Hence, the original distribution of the short-lived radon isotopes is preserved and can be determined after the removal of the chromatographic column by  $\gamma$ -spectroscopy, applying a HPGe-detector with a 1cm lead collimator. The result of such experiment is shown in Fig. 2.

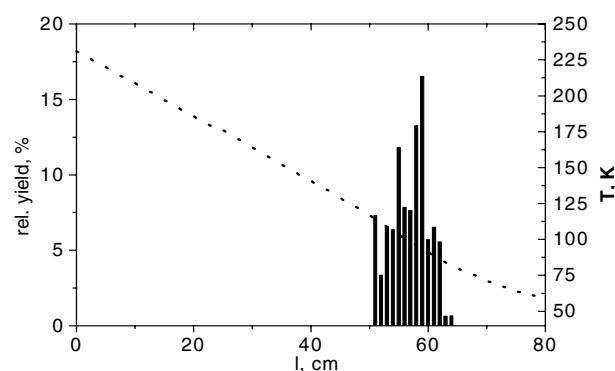


**Figure 2.** Vacuum thermochromatogram of  $^{219}\text{Rn}$  on a polycrystalline Ag surface treated by heating the metal in a reducing gas mixture of  $\text{H}_2/\text{N}_2$  at 1000 K. The temperature gradient is shown as a dotted line. Experiment lasted for 3 h.

A thermodynamic model [7,8] connects the isotope half-life, the dimensions of the column, the temperature gradient, the deposition temperature and the standard adsorption enthalpy ( $\Delta H_{\text{ads}}^{\circ}$ ) of the adsorbate (Rn) on the metal surface.  $\Delta H_{\text{ads}}^{\circ}$ -values for Rn on the investigated metal surfaces were deduced from the experimental results and are presented in Table 1.

**Table 1.** The standard adsorption enthalpies of Rn on transition metal surfaces determined by vacuum thermochromatography

Metal	$-\Delta H_{\text{ads}}^{\circ} / \text{kJ/mol}$
Cu	$37 \pm 2$
Ag	$20 \pm 2$
Au	$29 \pm 2$
Pd	$37 \pm 2$
Ni	$39 \pm 2$

## References

- [1] K. Pitzer, *J. Chem. Phys.* **63** (2), 1032 (1975).
- [2] B. Eichler, *Kernenergie* **19** (10), 307 (1976).
- [3] B. Eichler, *PSI Report 00-09*, (Villigen, 2000).
- [4] B. Grapengriesser et al., *Radiochim. Acta* **20**, 85 (1973).
- [5] G. Rudstam et al., *Radiochim. Acta* **20**, 97 (1973).
- [6] B. Eichler et al., *Kernenergie* **30**, 11 (1987).
- [7] H. Gäggeler et al., *Radiochim. Acta* **40**, 137 (1986).
- [8] B. Eichler, *Report ZfK-346*, (Rossendorf, 1977).

# A Monte-Carlo model of vacuum thermochromatography

Robert Eichler & Matthias Schädel (GSI Darmstadt)

Monte-Carlo simulation methods for the evaluation of standard adsorption enthalpies ( $\Delta H^{\circ}_{\text{ads}}$ ) of chemical species from their deposition temperatures in gas thermochromatography have been suggested by Zvara [1]. Here, we present a new microscopic, kinetic Monte-Carlo model of the gas adsorption process occurring in vacuum thermochromatography to determine  $\Delta H^{\circ}_{\text{ads}}$  from the measured deposition temperature of radon [2]. The model powerfully yields deposition temperatures and deposition widths of species with known or predicted  $\Delta H^{\circ}_{\text{ads}}$  in a cylindrical stationary phase with a temperature gradient applied in vacuum. It can be easily adapted to different simple macroscopic geometries of the stationary phases (e.g. rectangular channels). It can be applied to select the best design of vacuum thermochromatography set-ups. As an input the model needs: (i) the geometrical dimensions of the stationary phase (tube length and diameter), (ii) the half-life of the nuclide, (iii) the maximum phonon frequency of the stationary phase [3], (iv) the temperature gradient along the stationary phase, and (v) the assumed standard adsorption enthalpy of the adsorbate on the stationary phase. The mean time the atom remaining in the adsorbed state at a defined temperature is determined by a Frenkel-like Ansatz:

$$t_{\text{ads}} = 1/\nu_B \cdot \exp(-\Delta H^{\circ}_{\text{ads}}/R \cdot T) \quad (1)$$

The randomly selected lifetimes ( $\tau$ ) (according to the radioactive decay law with the half-life  $t_{1/2}$ ) and adsorption times ( $\tau_a$ ) are distributed exponentially:

$$P(\tau) = 1/\tau \cdot \exp(-\tau/t_{1/2}) \quad (2)$$

$$P(\tau_a) = 1/\tau_a \cdot \exp(-\tau_a/t_{\text{ads}}) \quad (3)$$

The solid angles ( $\phi$ ,  $\theta$ ) of desorption of an adsorbed atom from a surface into the vacuum are selected randomly with a probability distribution using a cosine law according to Knudsen [4], i.e., the probability of adsorption under the angle  $\phi$  or  $\theta$  is  $\cos(\phi)$  or  $\cos(\theta)$ , respectively. One of these solid angles ( $\phi$ ) determines the movement of the atom along the column; see Figure 1.

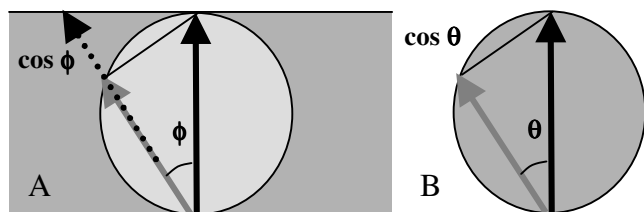


**Figure 1.** Schematic view of the trajectory of a desorbing atom in a cylindrical tube. Views perpendicular (A) and along (B) to the chromatographic column.

The sticking coefficient, which quantifies the adsorption probability of the adsorbate hitting the surface was set to be unity, as it was determined experimentally for the adsorption of Xe on metals [5]. The fates of about 10000 atoms each were calculated in this microscopic model, producing simulated internal thermochromatograms as shown in Figure 2 A and B (stepped lines). Simulations are repeated with different values

for  $\Delta H^{\circ}_{\text{ads}}$  until the simulated distribution matches best the experimentally determined activity distribution.

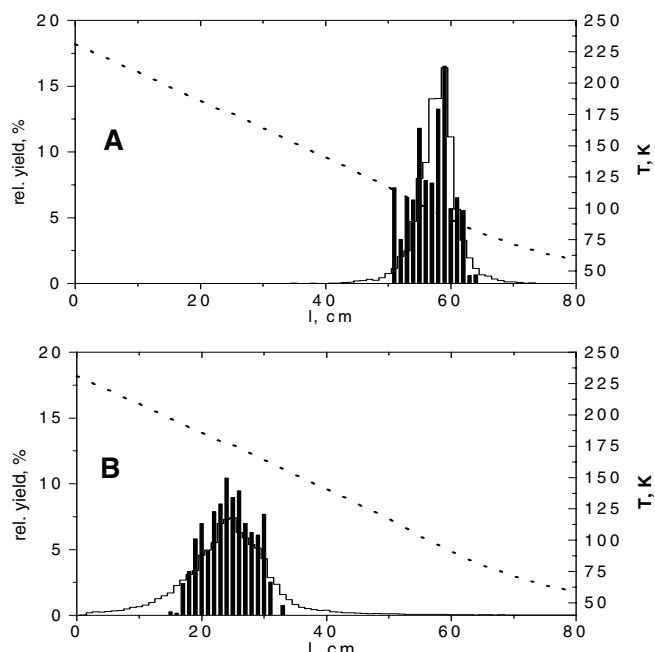


**Figure 2.** Experimentally observed vacuum thermochromatograms (bars) together with the obtained simulated thermochromatograms using the described model (stepped line). A:  $^{219}\text{Rn}$  on a polycrystalline Ag surface treated by heating the metal in a reducing gas mixture of  $\text{H}_2/\text{N}_2$  at 1000 K. B:  $^{220}\text{Rn}$  on a polycrystalline Ni surface treated by heating the metal in a reducing gas mixture of  $\text{H}_2/\text{N}_2$  at 1000 K. The temperature gradients are shown as dotted lines.

The resulting  $\Delta H^{\circ}_{\text{ads(kin)}}$  for the adsorption of Rn on different transition metals are listed in Table 1 together with the  $\Delta H^{\circ}_{\text{ads(therm)}}$  determined using a collective thermodynamic equilibrium model of adsorption [2]. Both values are in good agreement.

**Table 1** The standard adsorption enthalpies of Rn on transition metal surfaces determined using a well known thermodynamic collective model of vacuum thermochromatography and the microscopic model developed in this work

Metal	$-\Delta H^{\circ}_{\text{ads(therm)}} / \text{kJ/mol}$	$-\Delta H^{\circ}_{\text{ads(kin)}} / \text{kJ/mol}$
Cu	$37 \pm 2$	$40 \pm 2$
Ag	$20 \pm 2$	$23 \pm 2$
Au	$29 \pm 2$	$33 \pm 2$
Pd	$37 \pm 2$	$41 \pm 2$
Ni	$39 \pm 2$	$43 \pm 2$

## References

- [1] I. Zvara, *Radiochim. Acta* **38**, 95 (1985).
- [2] R. Eichler et al., this report and *J.Phys.Chem B* (submitted).
- [3] P.H. Dederichs et al., *Landoldt Börnstein: Metalle*, Bd. 13, Springer-Verlag: Berlin, Heidelberg, New York (1981).
- [4] M. Knudsen *Ann. Phys.* **4** **28**, 75 (1909).
- [5] P.W. Palmberg, *Surf. Sci.* **25**, 598, (1971).

# Prediction of adsorption enthalpies of the SHE 112 and 114 on transition metals

Robert Eichler & Matthias Schädel (GSI Darmstadt)

An empirical adsorption model for the adsorption interaction of light noble gases on metal surfaces is given by Miedema et al. [1]. It assumes a proportionality between the adsorption enthalpy ( $\Delta H_{\text{ads}}^{\circ}$ ) and the energy of adhesion ( $\Delta \gamma_{\text{ad}}(A,B)$ ). The energy of adhesion can be calculated using the surface energies ( $\gamma^{\circ}$ ) of the elements A (adsorbate) and B (surface) at 0 K [1] (see eqns.1 and 2).

$$\Delta \gamma_{\text{ad}}(A,B) = -2 \Phi (\gamma^{\circ}(A) \gamma^{\circ}(B))^{1/2} \quad (1)$$

$$\Delta H_{\text{ads}}^{\circ} = -0.71 \cdot 10^9 F \Phi V_A^{2/3} (\gamma^{\circ}(A) \gamma^{\circ}(B))^{1/2} \quad (2)$$

$\Phi$  ... dissimilarity parameter (calculated) [1]

$F$  ... geometrical factor (empirically 0.31) [1]

$V_A$  ... Volume of the spherical, adsorbed atom

A comparison of a large number of experimentally determined adsorption enthalpies for the light noble gases with such a calculation suggests [1], to calculate the adsorption enthalpies of the light noble gas elements Ne, Ar, and Kr by multiplying known adsorption enthalpies of Xe with empirical constant factors ( $C_x(Z,Xe)$ ); see eqn. 3. Recommended factors are compiled in the upper part of Table 1 for Ne, Ar, Kr and Xe.

$$\Delta H_{\text{ads}}^{\circ}(Z) = C_x(Z,Xe) \cdot \Delta H_{\text{ads}}^{\circ}(Xe) \quad (3)$$

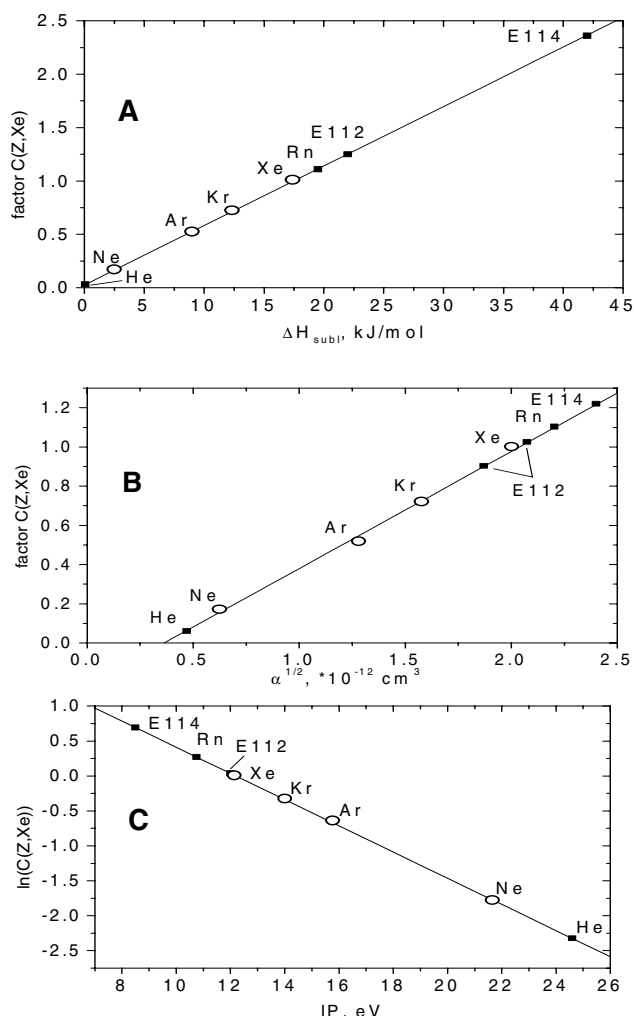


Figure 1. Empirical extrapolations of  $C_x(Z,Xe)$ .

Three different empirical correlations of  $C_x(Z,Xe)$  have been obtained from known properties of adsorbate atoms (circles in Figure 1, A-C): the enthalpy of sublimation ( $\Delta H_{\text{subl}}$ ), the polarizability ( $\alpha$ ), and the ionization potential (IP). The factors extrapolated for the noble gases He and Rn and for the hypothetical noble gas elements 112 and 114 (squares in Figure 1 A-C) are listed in the lower part of Table 1.

Table 1. Empirical factors  $C_x(Z,Xe)$  that connect the heat of adsorption of a closed shell atom,  $Z$ , with the known heat of adsorption of Xe on the same metallic substrate.

Element	$C_A(Z,Xe)$	$C_B(Z,Xe)$	$C_C(Z,Xe)$
Ne	0.17	0.17	0.17
Ar	0.52	0.52	0.52
Kr	0.72	0.72	0.72
Xe	1	1	1
He	0.032	0.12	0.098
Rn	1.11	1.11	1.31
E112	1.25	0.91	1.04
E114	2.36	1.2	2.00

As a test, adsorption enthalpies of Rn on different transition metals have been calculated with eqn. 3. They agree well with the experimental results from [2]; see Table 2. Even the trend in the adsorption interactions of Rn on the metals  $\text{Ag} < \text{Au} < \text{Pd} \leq \text{Ni}$  is well reproduced. The deviation of Cu is object of further investigations.

Table 2. Comparison of experimental [2] and calculated data for the adsorption of Rn on transition metal surfaces [2]

Metal	$-\Delta H_{\text{ads}}^{\circ}(\text{Exp}) / \text{kJ/mol}$	$-\Delta H_{\text{ads}}^{\circ}(\text{calc}) / \text{kJ/mol}$
Ag	$21 \pm 3$	$26 \pm 2$
Au	$31 \pm 3$	$33 \pm 2$
Pd	$39 \pm 3$	$35 \pm 2$
Ni	$41 \pm 3$	$37 \pm 2$
Cu	$38 \pm 3$	$25 \pm 2$

Assuming a fictitious noble gas behavior of the elements 112 and 114, we predict adsorption enthalpies on the transition metals Cu, Ag, Au, Pd, and Ni; see Figure 2.

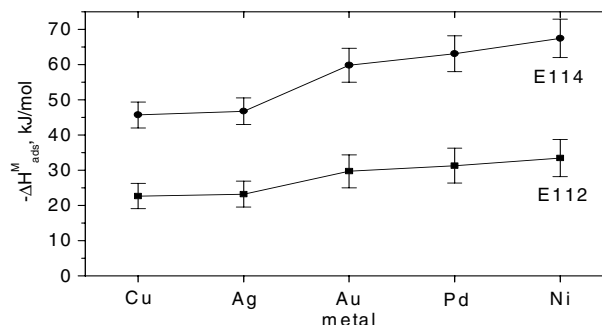


Figure 2. Predicted standard adsorption enthalpies of the hypothetical noble gas elements 112 and 114.

## References

- [1] A.R. Miedema et al., *Surf. Sci.* 104, 491 (1981).
- [2] R. Eichler et al., this GSI report, and *J.Phys.Chem B*, submitted 2001.

# Intermetallic Compounds of Element 112: the Electronic Structure and Bonding of HgX and 112X (X = Pd, Ag and Au)

V. Pershina<sup>1</sup>, T. Bastug<sup>2</sup>, T. Jacob<sup>2</sup>, B. Fricke<sup>2</sup>  
<sup>1</sup>GSI, Darmstadt

<sup>2</sup>Fachbereich Physik, Universität Kassel, 34109 Kassel

The next heaviest element which is to be studied chemically at the JINR, Dubna, [1] and GSI [2] is element 112. Its properties are expected to be unique: high volatility and inertness due to the very strong relativistic stabilization of the 7s electrons and the closed-shell configuration,  $7s^2 6d^{10}$  [3]. The surface of the chromatography column in the gas-phase chromatography experiments is to be made out of gold and palladium, since the interaction of Hg, the nearest homolog of element 112, with those metals was found to be rather strong [4].

To detect element 112 on those surfaces, the knowledge of its adsorption enthalpy is highly desirable. As a first step in the study of the metal-surface interaction, we have calculated here the electronic structure and bonding of the dimers, HgX and 112X (X = Pd, Ag and Au). The calculations were performed using the fully relativistic density-functional method (DFT) with the relativistic general gradient approximation (RGGA) for the exchange-correlation potential [5]. The Mulliken population analysis was applied additionally to study bonding in these systems. The calculated RGGA binding energies,  $D_e$ , optimized bond lengths,  $R_e$ , and harmonic frequencies,  $\omega$ , are shown in Table 1. The obtained  $D_e$  are probably too large by about 0.2 eV, which is an average error of the DFT method [5].

Table 1. Calculated RGGA binding energies,  $D_e$ , bond lengths,  $R_e$ , and harmonic frequencies,  $\omega$ , for HgX and 112X (X = Pd, Ag and Au)

Molecule	$R_e$ , Å	$D_e$ , kJ/mol	$\omega$ , cm <sup>-1</sup>
HgPd	2.56	61.2	125.62
HgAg	2.72	29.4	90.20
HgAu	2.66	52.7	101.95
112Pd	2.62	45.3	115.00
112Ag	2.76	19.0	75.41
112Au	2.73	31.7	79.17

Table 2. Overlap populations of the valence AO in HgAu and 112Au

Orbitals	HgAu	112Au
ns-ns	0.01	-0.02
ns-np <sub>1/2</sub>	0.04	0.05
ns-np <sub>3/2</sub>	0.06	0.03
np(tot)-ns	0.06	0.04
(n-1)d-np	0.01	0.00
(n-1)d-(n-1)d	-0.01	-0.01
OP(tot)	0.34	0.24

The calculations revealed an increase in  $R_e$  and a decrease in  $D_e$  of about 15 – 20 kJ/mol from HgX to 112X. The decrease in  $D_e$  is explained by a drastic relativistic stabilization and therefore

inertness of the  $7s^2$  shell. This results in a large decrease in the  $7s(112)$ -Au overlap compared to the  $6s(\text{Hg})$ -Au one, as the data of Table 2 show. The contribution of the other orbitals is almost unchanged.

In Fig. 1, the calculated  $D_e$  are shown together with experimental adsorption enthalpies,  $\Delta H_{\text{ads}}$ , of Hg on the corresponding metal surfaces [4]. One can see nice agreement for the trends between the two types of data, with the interaction of Hg and element 112 with Pd being the strongest.

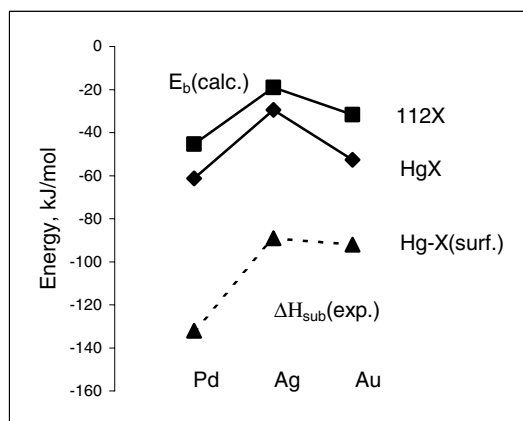


Fig. 2. Calculated binding energies for HgX and 112X (X = Pd, Ag and Au) and measured  $\Delta H_{\text{ads}}$  on the corresponding metal surfaces [4,6]

Thus, the calculations describe the bonding in the right way, so that the difference in  $D_e$  between HgX and 112X could be related to the difference in  $\Delta H_{\text{ads}}$  of Hg and element 112 on the metal surfaces. Thus, element 112 is expected to be weaker adsorbed than Hg, though not as weak as was expected earlier.

In the future calculations of adsorption on a cluster, one can foresee even a smaller difference between Hg and element 112, since the 6d orbitals of the latter will be more involved in the coordinated bonding due to their relativistic destabilization and expansion [3].

## References

- [1] A. Yakushev, presentation at the ASR2001, Tokai, Japan, 2001, to be published.
- [2] H. W. Gäggeler, et al. UNILAC Proposal, GSI, 2000.
- [3] B. Fricke, *Struct. Bond.* **21**, 89 (1975).
- [4] B. Eichler, H. Rossbach, *Radiochim. Acta* **33**, 121 (1983).
- [5] S. Varga et al. *Phys. Rev. A* **59**, 4288 (1999).
- [6] S. Soverna, et al. Presentation at the GDCh meeting, Würzburg, 2001.

# Towards a calculation of adsorption enthalpies for molecules of superheavy elements

C. Sarpe-Tudoran<sup>1</sup>, T. Jacob<sup>1</sup>, B. Fricke<sup>1</sup>, S. Fritzsche<sup>1</sup>, W.-D. Sepp<sup>1</sup>, V. Pershina<sup>2</sup>  
<sup>1</sup>Fachbereich Physik, Universität Kassel, 34109 Kassel  
<sup>2</sup>GSI, Darmstadt

In order to be able to calculate adsorption enthalpies for molecules of superheavy elements which can be measured in gas-phase thermochromatography experiments we are presently developing a code which should be able to calculate this quantity. Our starting-point was a full relativistic *ab initio* density functional molecular code [1]. In order to be able to simulate larger clusters which eventually represent the surface of a solid, our first approach was to generate a parallelized version so that clusters of up to 100 atoms can be calculated in reasonable times. This has now been achieved [2].

The cluster-size which is needed to reach convergence for the quantity of adsorption enthalpie is strongly dependent on the elements that are involved. As an example, to describe the adsorption of CO on Pt(111) about 20 Pt atoms are sufficient [3], whereas Al on Al(100) requires much more atoms [4, 5]. Especially those surfaces that are good conductors require a huge amount of atoms.

In addition to be able to calculate adsorption of molecules of superheavy elements a fully relativistic code is indispensable. To study the size convergence we present here cluster-size-dependent full relativistic calculations for the adsorption of Cu on Cu(100). We have chosen this system as a test because this allows a comparison with other (non-relativistic) calculations as well as copper is a well conducting element.

The method that is used for the calculations presented here is a relativistic four-component self-consistent field density functional approach. The total energy can be written as

$$E[\varrho] = T^S + E^N[\varrho] + E^C[\varrho] + E^{xc}[\varrho] \quad (1)$$

with the electronic density

$$\varrho(\vec{r}) = \sum_{-mc^2 < \varepsilon_i \leq \varepsilon_F} \psi_i^\dagger(\vec{r})\psi_i(\vec{r}). \quad (2)$$

Here the density is obtained from a sum of  $M$  auxiliary one-particle Dirac spinors. Then the corresponding relativistic form of the Kohn–Sham equations (rKS) [6] is

$$(\hat{t} + V^N(\vec{r}) + V^C(\vec{r}) + V^{xc}(\vec{r})) \psi_i(\vec{r}) = \varepsilon_i \psi_i(\vec{r}), \quad (3)$$

where  $\hat{t} = -ic\vec{\alpha} \cdot \vec{\nabla} + (\beta - 1)mc^2$  is the Dirac kinetic energy operator and  $V^N$  and  $V^C$  are the Coulomb potentials of the nuclei and the electrons.  $V^{xc}$  is the exchange-correlation potential and  $\varepsilon_i$  are the energy eigenvalues of the Dirac spinors.

During the self-consistent cycles the relativistic local-density approximation (rLDA) for the exchange-correlation functional is applied within the parametrization for the correlation suggested by Vosko, Wilk, and Nu-

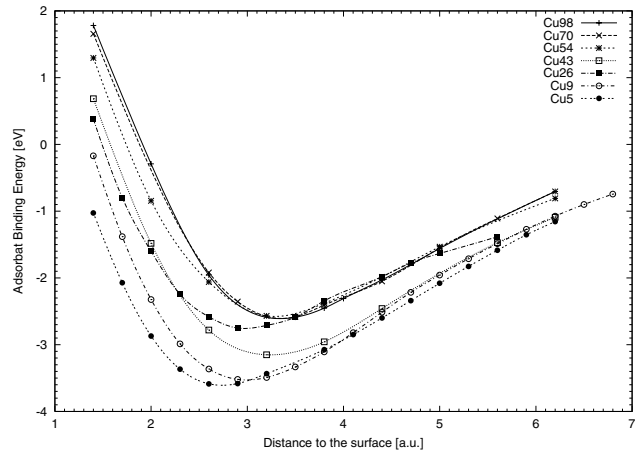


Figure 1: Potential energy curves in rLDA-approximation for all calculated systems.

sair [7]. Finally the total energy is calculated perturbatively with the relativistic forms of the generalized gradient approximation (rGGA) [8]. For the exchange we use Becke's [9] formulation and for the correlation the functional proposed by Perdew [10] (B88/P86).

After extensive calculations we are able to give the results for the potential energy curves as function of the distance of the adatom to the surface for system Cu<sub>5</sub> up to Cu<sub>99</sub> in Fig.1.

As can be seen from these curves the results are the same for Cu<sub>54</sub> and larger systems, so that the binding energy in the rLDA-approximation is -2.70 eV. This number can be compared to the best solid-state slab-calculations of Scheffler *et al.* [11] who got -2.74 eV.

This result is the first step towards a calculation of atoms respectively molecules of superheavy elements on realistic solids which will be needed in thermochromatography experiments.

## References

- [1] T. Bařtuř *et al.*, Phys. Rev. B **55**, 5015 (1997)
- [2] T. Jacob, PhD thesis, Universität Kassel (2001)
- [3] D. Geschke *et al.*, Phys. Rev. B, in press
- [4] R. Stumpf *et al.*, Phys. Rev. B **53**, 4958 (1996)
- [5] T. Jacob *et al.*, Surf. Sci. **486** (3), 194 (2001)
- [6] W. Kohn *et al.*, Phys. Rev. A **140**(4B), 1133 (1965)
- [7] S. H. Vosko *et al.*, Can. J. Phys. **58**, 1200 (1994)
- [8] E. Engel *et al.*, Phys. Rev. A **53**, 1367 (1996)
- [9] A. D. Becke, Phys. Rev. A **38**(6), 3098 (1988)
- [10] J. P. Perdew *et al.*, Phys. Rev. B **33**(12), 8800 (1986)
- [11] Y. Shin, M. Scheffler, private communications

# Theoretical Predictions of Hydrolysis and Complex Formation of Element 104, Rf, in HF and HCl Solutions

V. Pershina<sup>1</sup> and J. V. Kratz<sup>2</sup>

<sup>1</sup>GSI, Darmstadt

<sup>2</sup>Institut für Kernchemie, Universität Mainz, 55099 Mainz

The accumulated results on the extraction behaviour of element 104, Rf, from HF and HCl solutions have revealed quite a number of surprises and disagreements between separate measurements (for a review, see ref. [1]). Another open question was that of hydrolysis of Rf, where two types of experiments [2,3] revealed different trends for Zr, Hf and Rf. To clear those points, our theoretical research has been extended to the consideration of the above mentioned processes. Thus, we present here results of the calculations of the electronic structures of various hydrated, hydrolyzed and fluoride/chloride complexes of Zr, Hf, and Rf. On their basis, we predict stability and extraction of these complexes under the experimental conditions.

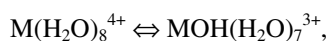
For the calculations, the fully relativistic density-functional (DFT) method [4] was used. For predictions of hydrolysis and complex formation, the model described in ref. [5] was utilized. It allows for predicting free energies of a reaction by calculating changes in the electrostatic,  $\Delta E^C$ , and covalent interactions, (overlap population, OP), separately using Mulliken numbers. Results of the calculations of  $E^C$  are shown in Table 1.

Table 1. Coulomb part of the binding energy,  $E^C$  (in eV), for various complexes of Zr, Hf and Rf.<sup>a</sup>

Complex	Zr	Hf	Rf
$M(H_2O)_8^{4+}$	-53.36(8.93)	-52.09(9.03)	-50.93(9.11)
$MOH(H_2O)_7^{3+}$	-58.05(8.10)	-56.70(8.21)	-55.04(8.29)
$MF(H_2O)_7^{3+}$	-53.36	-52.07	-50.53
$MF_2(H_2O)_6^{2+}$	-50.40 <sup>b</sup>	-49.14 <sup>b</sup>	-47.38 <sup>b</sup>
	-49.77 <sup>c</sup>	-48.56 <sup>c</sup>	-46.79 <sup>c</sup>
$MF_3(H_2O)_5^+$	-45.44	-44.20	-42.32
$MF_4(H_2O)_4$	-37.50	-36.25	-34.41
$MF_4(T_d)$	-12.79	-12.36	-11.61
$MF_6^{2-}$	-2.59	-1.18	0.23
$MCl_4(T_d)$	-5.37	-4.26	-3.28
$MCl_6^{2-}$	-1.21	0.41	2.13

<sup>a</sup> some OP are given in the parentheses; <sup>b</sup> cis-position, <sup>c</sup> trans-position of F atoms.

On the basis of the data of Table 1,  $\Delta E^C$  defining free energies of reactions, or complex formation constants, were determined. Thus, for the first hydrolysis step



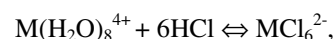
the values of  $\Delta E^C$  give the following trend in hydrolysis of group 4 elements: Zr > Hf > Rf in agreement with conclusions of ref. [3]. The first hydrolysis constant  $\log K_{11}(Rf) \approx -4$  was defined using  $\Delta E^C$ ,  $\Delta OP$  and  $\log K_{11}$  for Zr and Hf, similarly as it is shown in ref. [5].

For the fluorination process



the  $\Delta E^C$  data of Table 1 give different sequences for Zr, Hf and Rf depending on whether the fluorination process starts from the non-hydrolyzed, or hydrolyzed (fluorinated) species (i.e., depending on pH). Thus, in the first case, the trend is Zr > Hf > Rf for all types of complexes, while in the second case, the trend for the formation of the cationic complexes is the same, Zr > Hf > Rf, but it becomes reversed for the formation of the anionic  $MF_6^{2-}$ : Rf  $\geq$  Zr > Hf. The obtained sequences are in agreement with the cation exchange separations (CIX) of group 4 elements from 0.1 M  $HNO_3/10^{-3} - 10^{-1}$  M HF solutions [6], while for the anion exchange separations (AIX), the experimental sequence depends on the competition of the counter ion  $NO_3^-$  for the binding sites.

For the following chlorination process



i.e., for the AIX separations at 4-8 HCl, the trend will definitely be Zr > Hf > Rf, so that the sequence obtained in experiments [7] cannot be explained on the basis of the calculated data.

It is interesting to note here, that for the formation of the tetrahedral species,  $MF_4$  or  $MCl_4$ , which could be extracted, for example, by TBP, the trend is totally reversed in the group: Rf > Hf > Zr. Nevertheless, to predict the sequences in the extraction of these elements by TBP, the calculations of  $E^C$  for  $ML_4(TBP)_2$  would be desirable.

## References

- [1] J. V. Kratz, In *Heavy Elements and Related New Phenomena*, Ed. Greiner, W. and Gupta, Raj K., World Scientific: Singapore, 1999, p. 129-193.
- [2] A. Bilewicz, et al., *Radiochim. Acta*, **75**, 121 (1996).
- [3] K. R. Czerwinski, *Studies of Fundamental Properties of Rutherfordium (Element 104) Using Organic Complexing Agents*, Thesis, Lawrence Berkeley Laboratory, April 1992.
- [4] T. Bastug, et al., *Chem. Phys. Lett.* **211**, 119 (1993).
- [5] V. Pershina and J. V. Kratz, *Inorg. Chem.* **40**, 776 (2001).
- [6] E. Strub, et al., *Radiochim. Acta* **88**, 265 (2000).
- [7] Y. Nagame, presentation at the ASR2001, Tokai, 2001.